Unsteady effects on a pitching airfoil at conditions relevant for large vertical axis wind turbines

Unsteady effects on a pitching airfoil at conditions relevant for large vertical axis wind turbines

C E Brunner[1], J Kiefer[2], M O L Hansen[2] and M Hultmark[1]

[1] Department of Mechanical and Aerospace Engineering, Princeton University, Princeton, New Jersey, USA

[2] Department of Wind Energy, Technical University of Denmark, Kgs. Lyngby, Denmark

E-mail: cbrunner@princeton.edu

Abstract. Interest in offshore vertical axis wind turbines (VAWTs) has created a need to study VAWTs at much higher Reynolds numbers than they have previously been studied at. VAWTs are characterised by unsteady aerodynamics, and high Reynolds numbers have the potential to alter the blade aerodynamics significantly. Here, results are reported on an airfoil that is pitched sinusoidally around zero angle of attack at $Re_c = 1 \times 10^6$, at a reduced frequency $k = 0.15$ and amplitudes of $5^\circ \leq \hat{\alpha} \leq 20^\circ$. Since the static stall angle is not exceeded, no stall effects occur. Nevertheless, lift, drag and moment coefficients show noticeable hysteresis. Despite the high amplitudes of oscillation, lift and moment coefficients show reasonable agreement with unsteady aerodynamic theories by Theodorsen and Motta *et al.* with regard to the width of the hysteresis loops, but have noticeably steeper slopes.

1. Introduction

Vertical axis wind turbines (VAWTs) have several advantages compared to conventional horizontal axis wind turbines (HAWTs) [1]. They are agnostic to wind direction, have a simpler mechanical design, and have the potential to interact beneficially with each other when arranged in farms [2]. However, the aerodynamics of VAWTs are more complex than those of HAWTs, and cannot be approximated by steady one-dimensional models for optimisation and performance predictions. The non-dimensional parameters that characterise the aerodynamics of a VAWT are the Reynolds number, the tip speed ratio λ, and the solidity σ:

$$Re_D = \frac{U_\infty D}{\nu} \qquad \lambda = \frac{\omega D}{2U_\infty} \qquad \sigma = \frac{nc}{D}$$

Here, ν is the kinematic viscosity, U_∞ is the freestream velocity, D is the turbine diameter, ω is its angular velocity, c is the blade chord length, and n is the number of blades. The Mach number is assumed to be $Ma \leq 0.3$, so that compressibility effects are negligible.

Most VAWTs deployed to date are significantly smaller than commercial HAWTs. Modern offshore HAWTs have diameters up to 220 m and produce up to 12 MW [3]. In contrast, the largest VAWT deployed to date was 64 m in diameter [4], while most are much smaller. Nevertheless, the literature suggests that VAWTs have certain advantages over HAWTs particularly with regard to offshore applications [5]. Offshore VAWTs would be considerably larger and experience higher wind speeds than previously studied VAWTs, leading to significantly

higher Reynolds numbers. While most existing VAWTs operate at $Re_D \leq 3 \times 10^6$, offshore VAWTs might operate at $Re_D \geq 10^7$. This creates the need for detailed study of Reynolds number effects on the aerodynamic behaviour of VAWTs. In a recent experimental study, Miller *et al.* (2018) showed Reynolds number effects on the power coefficient up to $Re_D = 4 \times 10^6$ [6].

Studies of VAWT aerodynamics at the blade level can provide insight into such Reynolds number effects. The parameters that characterise an individual turbine blade are the Reynolds number based on the chord length and mean effective velocity, the reduced frequency k, the angle of attack α, the velocity ratio u_{rel}, and the aspect ratio AR:

$$Re_c = \frac{\overline{U_r}\, c}{\nu} \qquad k = \frac{\pi\, f\, c}{\overline{U_r}} \qquad u_{rel} = \frac{U_r}{U_\infty} \qquad AR = \frac{s}{c}$$

Here, U_r is the relative velocity seen by the blade, f is the pitching frequency of the airfoil, and s is the airfoil span. Since U_r changes throughout a rotation, Re_c and k are here defined as averages based on the mean relative velocity $\overline{U_r}$ following [7]. This blade-based parameterisation can be related to the turbine-based parameterisation as follows:

$$k = \frac{\sigma}{n} = \frac{c}{D} \qquad Re_c = \lambda\, \frac{c}{D}\, Re_D$$

The reduced frequency, k, which is a measure of the unsteadiness of the flow over the blade, is therefore solely a function of the turbine geometry. The angle of attack, α, and the velocity ratio, u_{rel}, are functions of λ and the azimuthal position of the blade θ. The exact relationship depends on the deceleration of the flow ahead of the turbine. In BEM-type models, this effect is captured by the local induction factor. There is no analytical expression for the velocity of the flow at the turbine, and thus no precise analytical expression for α and u_{rel}. However, they are often approximated by the following equations, in which the induction factor is assumed to be zero:

$$\alpha = tan^{-1}\left(\frac{sin\theta}{cos\theta + \lambda}\right) \qquad u_{rel} = \sqrt{1 + 2\,\lambda\, sin\theta + \lambda^2} \tag{1}$$

Thus, the amplitudes of the angle of attack oscillation $\hat{\alpha}$ and of the velocity ratio u_{rel} are solely a function of λ.

Unsteady effects are known to occur in both attached and separated flow conditions. The most prevalent unsteady effect is dynamic stall, which occurs when the angle of attack rapidly exceeds the stall angle. This sudden increase in angle of attack leads to the formation of a leading edge vortex which then convects downstream, causing a temporary increase in the lift force before it drastically collapses [8]. This phenomenon affects not only the performance, but also the structural integrity of the turbine.

Even if the blades do not exceed the stall angle at any point during their trajectory, unsteady phenomena still occur. Theodorsen developed analytical expressions for the time-dependent lift and moment coefficients of a flat plate pitching and heaving at small amplitude in a potential flow [9]. They account for added mass and shedding of vorticity into the wake. For the purpose of this study, pure pitching motion will be considered. Following [10], the equations for the lift and quarter-chord moment coefficients of an airfoil pitching sinusoidally around its half-chord are as follows:

$$C_{L,th} = \pi\,(2\,C(k)\,sin(\omega t) + k\,(C(k)+1)\,cos(\omega t)) \tag{2}$$

$$C_{M,th} = -\pi\left(\frac{k}{2}\,cos(\omega t) + \frac{k^2}{16}\,sin(\omega t)\right) \tag{3}$$

Here, $C(k)$ is the lift deficiency factor. The equations given are exact only for a flat plate oscillating at small angles of attack in an inviscid flow. Nevertheless, they have shown reasonable

agreement with experimental data of pitching thin airfoils [11] [12]. Motta *et al.* studied the effect of airfoil thickness on the unsteady lift and moment coefficients of a pitching airfoil and find that below an inversion point in the reduced frequency, an increase in thickness leads to an increase in hysteresis, whereas above the inversion point the trend is reversed [13]. The inversion point is itself a function of airfoil thickness. They modified the Theodorsen model to include an empirical correction for arbitrary airfoil thickness which modifies equations 2 and 3 as follows:

$$C_{L,mot} = \pi \left(2\, PL_3(c)\, C(k)\, sin(\omega t) + k \left(PL_1(c)\, C(k) + PL_4(c)\right) cos(\omega t)\right) \tag{4}$$

$$C_{M,mot} = -\pi \left(PM_1(c)\, \frac{k}{2}\, cos(\omega t) + PM_2(c)\, \frac{k^2}{16}\, sin(\omega t) \right) \tag{5}$$

Expressions for the $PL(c)$, $PM(c)$, and $C(k)$ are given in [13]. Most experimental studies of unsteady lift and moments on airfoils in attached flow are limited to amplitudes of oscillation below $\hat{\alpha} = 10°$.

Both numerical simulations and analytical models can be applied to capture the aerodynamic behaviour and performance of VAWTs. However, they often require tabulated airfoil data as inputs. Large Eddy Simulations (LES) can provide detailed accounts of the flow field, but are computationally intensive, especially at high Reynolds numbers [14]. To reduce the computational power required, LES is often combined with a blade level model that requires a lookup table. The most commonly applied analytical model is the double multiple streamtube model, a BEM-type model that uses momentum theory and an aerodynamic force analysis to iteratively solve for spatially-resolved induction factors, with significantly less computational effort [15]. The tabulated airfoil data are generally taken from steady airfoil experiments in which Re_c, the airfoil section and its angle of attack are matched, e.g. [16]. Such data do not account for unsteady effects on the blades due to the oscillating angle of attack and inflow velocity. Instead, corrections are often applied to account for dynamic stall effects at high amplitudes of oscillation [17].

Under what conditions a VAWT experiences dynamic stall as opposed to attached flow unsteady effects is the subject of ongoing investigations. The static stall angle α_{ss} depends on Re_c, the blade profile, and its aspect ratio AR, while the amplitude of oscillation $\hat{\alpha}$ depends on λ and the induction factor a. The occurrence of stall effects therefore likely depends on all of these variables. They are presumably less likely to occur at high α_{ss} and low $\hat{\alpha}$, i.e. at high Re_c, on thick blades with low AR, at high λ, and high a. Ferreira *et al.* state that dynamic stall generally occurs for $\lambda \leq 5$ [18], whereas Buchner *et al.* find that at $7 \times 10^4 \leq Re_c \leq 14 \times 10^4$ no leading edge separation occurs for $\lambda \geq 3.5$ [7]. With regard to the design of offshore VAWT, the nature of unsteady effects at high Re_c in particular requires further study.

The present study captures the unsteady effects on a VAWT blade at high Reynolds number. Experiments were conducted in a pressurised wind tunnel, enabling high Reynolds numbers without the need for high velocities or large models. A pitching airfoil with a NACA 0021 profile was studied at $Re_c = 1 \times 10^6$ and $k = 0.15$. The freestream velocity was held constant over the cycle. The airfoil was pitched at varying amplitudes around a mean angle of $\alpha_0 = 0°$. While the angle of attack variation of a VAWT blade is given by equation 1, it was approximated as sinusoidal following [19]. In all cases, the amplitude of oscillation was below the static stall angle of the airfoil at this Reynolds number, and corresponded to tip speed ratios of $\lambda \geq 2.9$. The attached flow hysteresis in lift and moment coefficients were compared to the models by Theodorsen [9] and Motta *et al.* [13].

2. Methodology

Experimental data were obtained in the High Reynolds number Test Facility (HRTF) at Princeton University, a closed-loop wind tunnel that can achieve pressures up to 230 atm and

Table 1. Individual experimental runs in the pressurised High Reynolds number Test Facility at Princeton University. In all cases $Re_c = 1.00\,(\pm 0.01) \times 10^6$ and $k = 0.15 \pm 0.01$.

$\hat{\alpha}$	$P[MPa]$	$U_\infty[m/s]$	$f[Hz]$	# of cycles	points/cycle
5°	4.00	2.27	0.62	1550	3.2×10^4
10°	4.21	2.17	0.65	1495	3.1×10^4
15°	9.24	1.05	0.32	512	6.3×10^4
20°	10.00	0.99	0.28	504	7.1×10^4

velocities up to 10 m/s. The test section is 4.88 m in length and has a circular cross-section with a diameter of 0.49 m. Density is a strong function of pressure whereas the dynamic viscosity is only a very weak function of pressure. Therefore, the use of pressurised air as the working fluid allows for high Reynolds numbers at low velocities. The freestream velocity is held constant throughout every experimental run. At a given pressure, the appropriate velocity is selected to achieve a desired Re_c. The frequency, f, is then determined based on the desired k. The parameters of the experimental runs presented here are shown in table 1. High amplitude experiments are conducted at high pressures and low velocities to ensure that f is low.

A NACA 0021 airfoil was chosen as the test model, allowing for convenient comparisons with existing experimental data of VAWTs from both laboratory and field experiments. The studies of [6] and [20] both use this section, and many other studies use moderately thick symmetric NACA airfoils [18]. The airfoil has a chord length of $c = 0.17$ m and an aspect ratio of $AR = 1.5$. Endplates are used to reduce three-dimensional effects. Their dimensions are described by equation 6, where $a_l = -\frac{76}{170}$, $a_t = \frac{144}{170}$ and $b = \frac{6}{17}$. A supporting rod suspends the wing model in the tunnel such that the two endplates are equidistant from the tunnel walls. The diameter of the supporting rod is 4 cm, and it is connected to the airfoil via a 1 cm thick circular base plate with a diameter of 8.5 cm. The center of rotation is at the half-chord.

$$y(x) = \begin{cases} \pm b\sqrt{1 - \frac{x^2}{a_l^2}}, & x \in [a_l, 0] \\ \pm b\sqrt{1 - \frac{x^2}{a_t^2}}, & x \in [0, a_t] \end{cases} \tag{6}$$

The airfoil is equipped with 32 pressure taps, which provide the pressure distribution around the surface of the airfoil. A force balance records lift, drag and moments on the airfoil. Generally, the force balance provided higher quality measurements than the pressure transducers at the low pressures and velocities used in this study. Thus, all data presented here were calculated using the force balance measurements. The sampling frequency was 20 kHz in all cases. Phase-averaged quantities were computed from all available cycles. The number of cycles for each run, as well as the number of data points per cycle are given in table 1. The accuracies of the pressure, density, and viscosity measurements are given in [6], and correspond to a systematic error of $\pm 0.97\%$ in Re_c and $\pm 0.4\%$ in k. Slight variations in Reynolds number up to $\pm 7.3\%$ occurred throughout an experimental run due to slight changes in temperature and pressure inside the tunnel. The force balance used was a JR3 multi-axis load cell with a manufacturer-provided range of 200 N with an accuracy of ± 0.5 N for the forces, and a range of ± 25 Nm with an accuracy of 0.0625 Nm for the moments. Because the experimental setup was designed for much higher Reynolds numbers, the forces recorded by the force balance were small compared to its range. However, zeroes were subtracted to account for any systematic offsets, and phase averaging was applied to reduce random fluctuation, so that the true error is likely much smaller than the manufacturer-provided accuracies suggest. While some scatter

Table 2. Conversion from $\hat{\alpha}$ to λ for all tested amplitudes using two exemplary induction factors a. In reality, a is a function of azimuthal position β.

$\hat{\alpha}$	$\lambda(a = 0)$	$\lambda(a = 0.25)$
20°	2.9	2.2
15°	3.9	2.9
10°	5.7	4.3
5°	11.5	8.6

in the data is expected due to variations in the flow between cycles, the predominant source of random error in this setup is electrical noise in the measuring equipment. Electrical noise is not expected to affect the phase-averaged quantities as long as they are fully converged. All data were filtered before phase averaging, and subsequently smoothed to achieve better convergence. However, the measurements of C_d and C_m at $\hat{\alpha} = 5°$ appear to not be fully converged. The exact uncertainty in the experimental setup is currently unknown and will be the subject of future investigation. The drag due to the supporting rod and the end plates was not subtracted, so that the drag coefficients reported should be considered to have an unknown offset. However, hysteresis behavior should be qualitatively correct.

The airfoil was oscillated sinusoidally around a mean angle of attack, α_0, using a stepper motor. The reduced frequency was held constant across all experimental runs at $k = 0.15$. This corresponds to a VAWT chord-to-diameter ratio of approximately 1:7. Equation 1 suggests that both the angle of attack and the relative velocity of a VAWT blade vary quite drastically at low tip speed ratios. For example, at $\lambda = 2$, the angle of attack amplitude is $\hat{\alpha} = 30°$, and the amplitude of velocity oscillation is $\hat{U_r} = 0.447\,\overline{U_r}$. However, these calculations do not account for variations in induction factor. A non-zero induction factor reduces $\hat{\alpha}$ corresponding to any given λ, or conversely reduces the λ corresponding to any given $\hat{\alpha}$. In a comparison of VAWT models, Ferreira *et al.* found induction factors to be as high as $a = 0.25$ on the front side and $a = 0.60$ on the back side of the turbine [21]. As a result, the angle of attack was shown not to exceed $\alpha = 10°$ on the front side and $\alpha = -5°$ on the back side. Table 2 provides a general idea of which λ correspond to the $\hat{\alpha}$ used in this study by considering two exemplary values of a. In reality, a is a function of azimuthal position β. The expected oscillations in wind speed, which according to equation 1 range from $\hat{U_r} = 0.087\,\overline{U_r}$ for $\hat{\alpha} = 5°$ to $\hat{U_r} = 0.326\,\overline{U_r}$ for $\hat{\alpha} = 20°$, were neglected because the current experimental setup does not allow for periodic variations in tunnel wind speed.

The experimental data is compared to the analytical predictions of Theodorsen [9] and Motta *et al.* [13]. Despite the use of endplates, the low AR of the airfoil lead to a shallower lift curve slope $\frac{\partial C_l}{\partial \alpha}$ and a higher stall angle α_{ss} than is expected for a 2D airfoil. Furthermore, the finite cross-section of the wind tunnel and associated blockage effects lead to a steeper $\frac{\partial C_l}{\partial \alpha}$ and a higher $C_{l,max}$. Existing corrections were developed for steady flows, and their validity for unsteady flows is unclear. Furthermore, no established blockage corrections for wind tunnels with round cross-sections are known to the authors. Therefore, no corrections were applied to the data presented here. The analytical predictions of Theodorsen and Motta *et al.* are based on thin airfoil theory and therefore assume a static lift curve slope of $\frac{\partial C_l}{\partial \alpha} = 2\pi$. In order to compare these 2D theories to the experimental data, an aspect ratio correction described by [22] was applied in reverse. However, the use of the geometric aspect ratio $AR_g = 1.5$ in the correction did not project the potential flow lift curve $C_l = 2\pi\alpha$ onto the experimental static lift curve. This is likely due to the presence of the endplates and blockage effects. Therefore, in order to provide an accurate

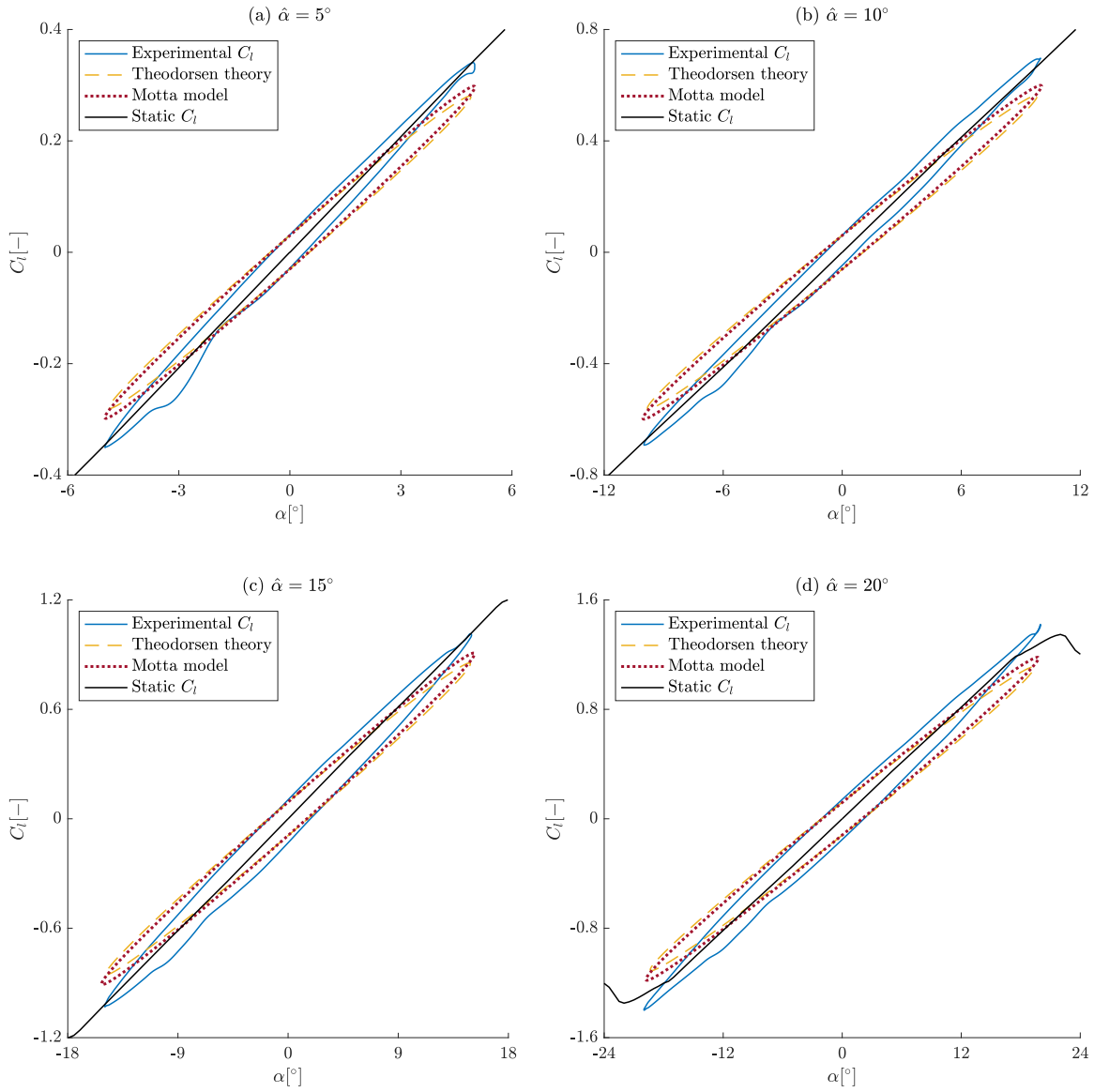

Figure 1. Lift coefficient for a NACA 0021 airfoil sinusoidally pitching around a zero mean angle of attack at reduced frequency $k = 0.15$ and $Re_c = 10^6$. Note the differing axis scales.

comparison between the 2D theories and the experimental data, the effective aspect ratio used for the correction was empirically selected such that the correction projected $C_l = 2\pi\alpha$ onto the experimentally obtained steady lift curve. Thus, the aspect ratio used for the correction was $AR_e = 2.8$, and the correction should be regarded as purely empirical.

3. Results

Due to the high Reynolds number and the relatively low aspect ratio of the wing model, the static stall angle $\alpha_{ss} = 21°$ is higher than in most VAWT studies reported in the literature. In steady conditions, at $Re_c = 1 \times 10^6$, the maximum lift coefficient, attained at α_{ss}, was $C_{L,max} = 1.31$. The airfoil began to stall gradually from the trailing edge starting at around 20°. Thus, even

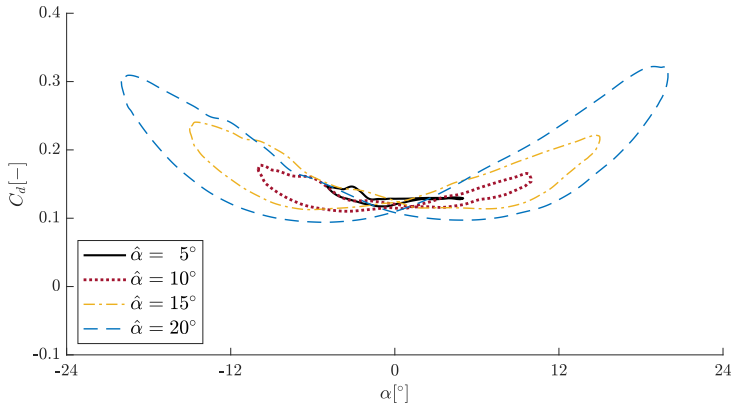

Figure 2. Drag coefficient for a NACA 0021 airfoil sinusoidally pitching around a zero mean angle of attack at reduced frequency $k = 0.15$ and $Re_c = 10^6$. Drag due to supporting rod was not subtracted, so values are purely qualitative

at the highest amplitude of oscillation tested here, $\hat{\alpha} = 20°$, the airfoil does not enter the stall regime at any point during the oscillation.

Figure 1 shows the lift coefficient, C_l, as a function of angle of attack for the various amplitudes tested. No stall effects are visible, as expected. For all tested amplitudes, the lift coefficient follows a clockwise hysteresis loop. Despite the high amplitudes of oscillation no amplitude-dependent changes in the shape of the hysteresis loop are visible. Furthermore, the width of the hysteresis loop appears to agree with the theoretical predictions. Motta *et al.* predicted that for k larger than the phase inversion point at $k_i = 0.144$, added mass effects will dominate over the circulatory contribution, causing a clockwise hysteresis loop [13]. At the inversion point, no hysteresis is predicted to occur. The present study was conducted just above the phase inversion point at $k = 0.15$. Thus, the clockwise hysteresis loops observed are consistent with the theory. Above the inversion point, an increase in airfoil thickness is predicted to reduce the width of the hysteresis loop. However, figure 1 indicates that this effect is small, if at all present. The experimental data show a steeper loop, leading to a maximum C_l as high as the static C_l at those angles. Both Theodorsen and Motta et al. predict a decrease in C_l compared to the static condition. This decrease is due the lift deficiency factor $C(k)$, which accounts for the shedding of vorticity into the wake. The experimental data suggests that this effect might be overestimated for the conditions studied here.

The drag coefficient is shown as a function of angle of attack in figure 2. The drag measurements were obtained using the force balance, and the drag due to the supporting rod was not subtracted. Since the supporting rod is cylindrical, we expect no additional drag hysteresis due to its presence. As such, the absolute drag values will not represent the drag on the airfoil, but have an unknown offset. However, we expect the characteristics of the drag hysteresis loop to be representative of the airfoil. As with the lift coefficient, the drag coefficient follows a hysteresis loop that widens as $\hat{\alpha}$ increases, where the drag is higher as the angle moves away from zero and lower as it returns to zero. Both the qualitative shape and the direction of the drag curve are in agreement with those found by Leishman and Beddoes at angles below the stall angle [11]. In fact, they found that the pressure drag became negative on the downstroke. The models by Theodorsen and Motta *et al.* do not predict drag.

The moment coefficient around the quarter chord point, $C_{m,\frac{c}{4}}$, shows significant counter-clockwise hysteresis. While the experimental data at $\hat{\alpha} = 5°$ is not fully converged and therefore cannot be reliably compared with the analytical predictions, the moment coefficients at higher

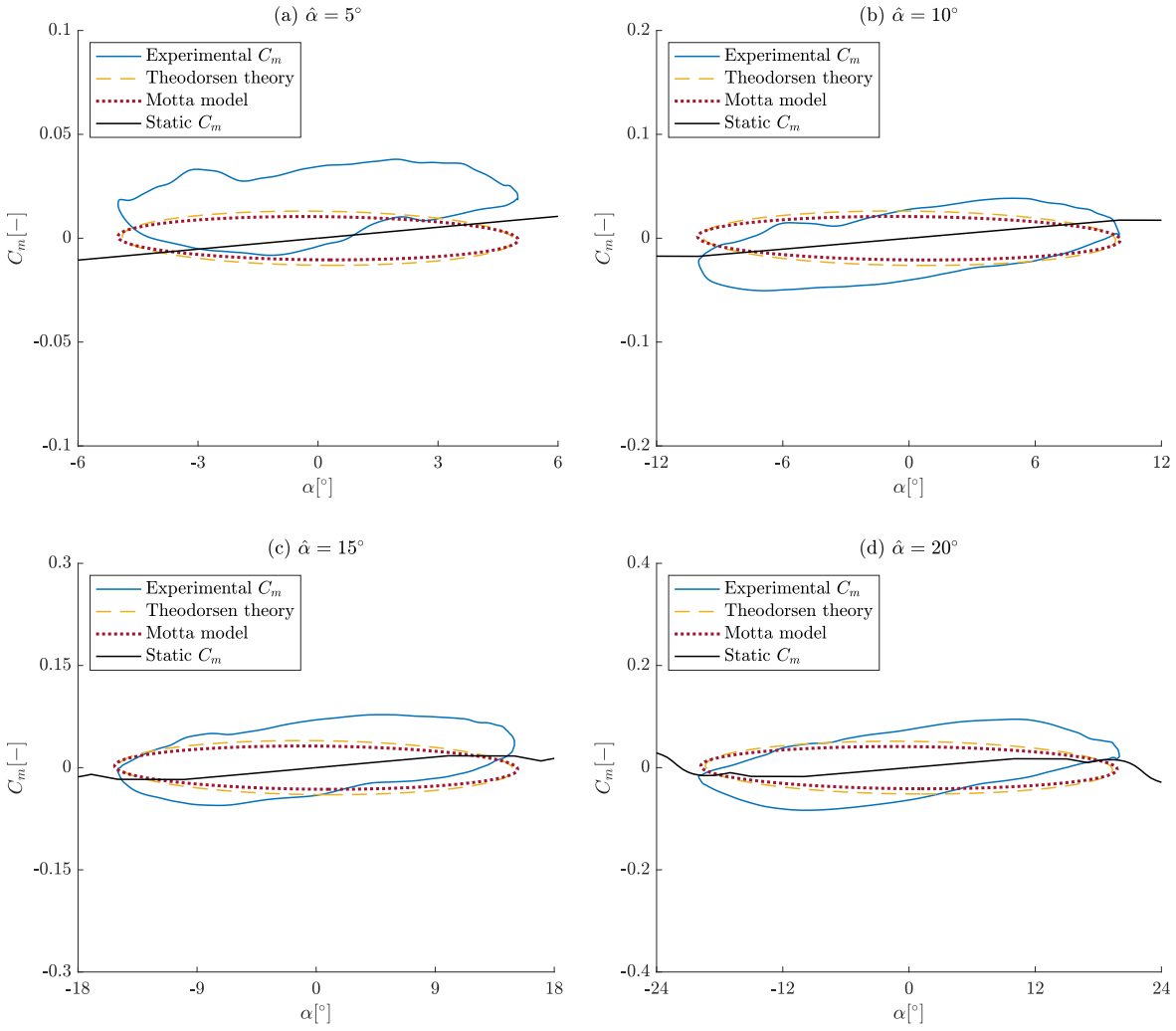

Figure 3. Moment coefficient around the quarter-chord for a NACA 0021 airfoil sinusoidally pitching around a zero mean angle of attack at reduced frequency $k = 0.15$ and $Re_c = 10^6$

amplitudes of oscillation show an asymmetry that is not predicted by either of the theories. The magnitude of C_m appears to be lower as the angle moves away from zero than when it returns to zero. The aerodynamic center of a symmetric airfoil in attached flow is assumed to lie at the quarter-chord point. Because of this, $C_{m,\frac{c}{4}}$ is assumed to be zero in steady attached flow, and in unsteady conditions causes the moment coefficient to depend purely on the added mass effect. Motta *et al.* point out that this causes the theoretical predictions to diverge slightly from experimental data, since the aerodynamic center of an airfoil of finite thickness is not exactly at the quarter-chord point. Here, the steady moment coefficient is shown to increase slightly with increasing angle of attack. This might explain the slight upward slope in the unsteady experimental C_m curves.

4. Conclusion

Lift, drag and moments on a pitching symmetric airfoil were studied at pitch amplitudes of $5° \leq \hat{\alpha} \leq 20°$. A high pressure facility was used to achieve both high Reynolds number

($Re_c = 10^6$) and unsteady conditions. Even at the highest amplitudes tested, no stall effects were observed, since the angle of attack never exceeded the static stall angle of $\alpha_{ss} = 21°$. Nevertheless, unsteady effects lead to hysteresis in the lift, drag and moment coefficients. The lift and moment coefficients showed reasonable agreement with unsteady aerodynamic theories by Theodorsen and Motta *et al.* regarding the widths of the hysteresis loops, but showed steeper slopes.

As Reynolds number and thus static stall angle are increased, dynamic stall is delayed to higher angles of attack, and thus to lower tip speed ratios. Instead, attached flow unsteady effects cause the aerodynamic coefficients to differ noticeably from their steady state values. The data presented here suggests that the theories developed for and validated at small amplitudes of oscillation could be extended to larger amplitudes in order to model unsteady blade loading on VAWTs operating at high Reynolds numbers. Further studies are necessary to characterise the effects of increasing Reynolds number on VAWT aerodynamics.

Acknowledgments

This work was funded by the United States National Science Foundation under grant CBET 1652583, and by the United States National Defense Science and Engineering Graduate Fellowship. The authors would like to thank Dan Hoffman at the Princeton Gas Dynamics Laboratory for his great help and advice in setting up the experiment.

Contributions

JK designed and built the airfoil setup. CEB conducted the experiments. JK and CEB analyzed the data. CEB wrote the manuscript. All authors reviewed the paper. MH and MOLH provided scientific advice and supervised the research.

References

[1] Sutherland H J, Berg D E and Ashwill T D 2012 A retrospective of VAWT technology. *Sandia National Laboratories Tech. Report SAND2012-0304*
[2] Dabiri J O 2011 Potential order-of-magnitude enhancements of wind farm power density via counter-rotating vertical axis wind turbine arrays *J. Renew. Sustainable Energy* **3** 44–50
[3] GE renewable energy. Haliade-X offshore wind turbine platform. Web accessed 03/02/2020
[4] Paraschivoiu I 2002 *Wind turbine design: with emphasis on darrieus concept* Quebec, Canada
[5] Griffith D T, Barone M, Paquette J, Owens B, Bull D, Simao Ferreira C, Goupee A and Fowler M Design studies for deep-water floating offshore vertical axis wind turbines *Sandia National Laboratories Report*
[6] Miller M A, Duvvuri S, Brownstein I, Lee M, Dabiri J O and Hultmark M 2018 Vertical-axis wind turbine experiments at full dynamic similarity *J. Fluid Mech.* **844** 707–20
[7] Buchner A J, Soria J, Honnery D and Smits A J 2018 Dynamic stall in vertical axis wind turbines: scaling and topological considerations *J. Fluid Mech.* **841** 746–66
[8] McCroskey W J 1981 The phenomenon of dynamic stall *NASA Tech. Memorandum 81264*
[9] Theodorsen T 1935 General theory of aerodynamic instability and the mechanism of flutter *NACA Tech. Report 496* 413–33
[10] Katz J and Plotkin 2001 *Low-speed aerodynamics* 2nd ed. New York, NY, USA
[11] Leishman J G and Beddoes T S 1986 A semi-empirical model for dynamic stall *J. Am. Helicopter Soc.* **34** 3–17
[12] Dyachuk E, Rossander M, Goude A and Bernhoff H 2015 Measurements of the aerodynamic normal forces on a 12-kW straight-bladed vertical axis wind turbine *Energies* **8** 8482-96
[13] Motta V, Guardone A and Quaranta G 2015 Influence of airfoil thickness on unsteady aerodynamic loads on pitching airfoils *J. Fluid Mech.* **774** 460–87
[14] Hezaveh S, Bou-Zeid E, Lohry M W and Martinelli L 2017 Simulation and wake analysis of a single vertical axis wind turbine *Wind Energ.* **20** 713–30
[15] Paraschivoiu I 1987 Double-multiple streamtube model for studying vertical-axis wind turbines *J. Propulsion* **4** 370–7

[16] Sheldahl R E and Klimas P C 1981 Aerodynamic characteristics of seven symmetrical airfoil sections through 180-degree angle of attack for use in aerodynamic analysis of vertical axis wind turbines *Sandia National Laboratories Tech. Report SAND-80-2114*
[17] Gormont R E 1973 A mathematical model of unsteady aerodynamics and radial flow for application to helicopter rotors *USAAMRDL Tech. Report 72-67*
[18] Simao Ferreira C, van Kuik G, van Bussel G and Scarano F 2009 Visualization by PIV of dynamic stall on a vertical axis wind turbine *Exp. Fluids* **46** 97–108
[19] Dunne R and McKeon B J 2014 Dynamic separation on a pitching and surging airfoil as a model for flow over vertical axis wind turbine blades *32nd AIAA Applied Aerodynamics Conference*
[20] Bianchini A, Balduzzi F, Ferrara G, Persico G, Dossena V and Ferrari L 2019 A critical analysis on low-order simulation models for darrieus vawts: how much do they pertain to the real flow? *J. Eng. Gas. Turb. Power* **141** 011018
[21] Simao Ferreira C, Aagaard Madsen H, Barone M, Roscher B, Deglaire P and Arduin I 2014 Comparison of aerodynamic models for vertical axis wind turbines *J. Phys.: Conf. Series* **524** 012125
[22] Jacobs E N and Anderson R F 1931 Large-scale aerodynamic characteristics of airfoils as tested in the variable density wind tunnel *NACA Tech. Report NACA-TR-352*